Proceedings of the
Annual Stability Conference
Structural Stability Research Council
Atlanta, Georgia, April 21-24, 2020

Seismic response predictions from 3D steel braced frame building simulations

Hamid Foroughi[1], Gengrui Wei[2], Shahabeddin Torabian[3],
Matthew R. Eatherton[4], Benjamin W. Schafer[5]

Abstract

The seismic performance of steel building systems can be assessed through material and geometric nonlinear dynamic analysis. Extensive efforts have been conducted in the past, employing 2D building models, and incremental dynamic analysis to predict the collapse probability of steel building systems to earthquake excitation and justify seismic response modification coefficients (e.g., R) employed in equivalent lateral force-based design procedures. Little work has been performed on 3D building models where the vertical lateral force resisting system (LFRS) may interact with the building diaphragm. Here we examine two common steel braced frame vertical LFRSs: buckling restrained braces (BRBs) with their quite high R value, and concentrically braced frames (CBFs) with a more modest R. These vertical systems are coupled with a variety of alternative concrete-filled steel deck floor and bare steel deck roof diaphragms and 3D building simulations of the resulting 4 story steel frame buildings are conducted. The building layout is regular, but with a relatively high aspect ratio to place increased demands on the diaphragm. The models indicate interaction between the vertical LFRS and the diaphragm, and provide a means to understand the degree of conservatism inherent in existing and proposed diaphragm design methods. The role of P-Δ demands in the large deflection response of the buildings is highlighted.

1. Introduction

Seismic performance of buildings depend on both the vertical lateral force resisting system (LFRS), such as braced frames, and the horizontal LFRS, such as the roof or floor diaphragm. Conventional seismic design of buildings assumes that the vertical LFRS, e.g. a concentrically braced frame (CBF) or buckling restrained brace (BRB) frame, is the only source of inelastic action and hysteretic energy dissipation in the structure. However, it has been shown that diaphragms designed using traditional design procedures may be subject to inelasticity even during design level earthquakes (Rodriguez et al. 2007), and in the extreme may experience collapse such as happened for several concrete parking garages with precast concrete diaphragms during the 1994 Northridge earthquake (EERI 1996). The role of the diaphragm in energy dissipation may be

[1] Graduate Research Assistant, Johns Hopkins University, <hforoug1@jhu.edu>
[2] Graduate Research Assistant, Virginia Tech, <gwei1@vt.edu>
[3] Associate Research Scientist, Johns Hopkins University, <torabian@jhu.edu >
[4] Associate Professor, Virginia Tech, <meather@vt.edu >
[5] Professor, Johns Hopkins University, <schafer@jhu.edu>

particularly pronounced for single-story structures when the story stiffness is far greater than the in-plane diaphragm stiffness – a condition that can happen in steel buildings with braced frames and bare steel deck roof diaphragms.

Today in U.S. seismic design provisions, i.e. ASCE 7-16 (ASCE 2016), two different design methodologies exist for the seismic design of diaphragms. Traditional diaphragm design procedures assume the diaphragm demands are reduced by the response modification factor, R, which is associated with the vertical system alone. While, in the new alternative diaphragm design procedures, currently only applicable to concrete and wood diaphragms, a diaphragm response modification factor, R_s, is employed to reduce (or increase) the diaphragm demands based on the ductility and overstrength of the diaphragm alone. Today, there is no agreed upon R_s factor for bare steel deck or concrete-filled steel deck diaphragms.

Equivalent lateral force (ELF) based design in ASCE 7-16, irrespective of the diaphragm design details, does not emphasize the impact of geometric nonlinearity in assessment of the building – and is not well aligned with modern frame stability methods such as the Direct Analysis Method promoted in U.S. steel standards (AISC 360-16). Important questions related to the seismic performance of steel frames are (a) the impact of changes in the diaphragm design on the building response and (b) the impact of geometric nonlinearity on the response. In this paper these questions are explored through the design of BRB and CBF building archetypes with various diaphragm design options and analysis of the building archetypes with geometric nonlinearity. Nonlinear static pushover analyses and response history analyses using 44 ground motions scaled to three hazard levels are performed to study the behavior and seismic performance of the buildings.

2. Design and Modeling of Steel Building Archetypes

A series of detailed three-dimensional building archetypes have been developed for the Steel Diaphragm Innovation Initiative (SDII) as reported in Torabian et al. (2017). Here a subset of these buildings are selected for detailed study. First, the basic building design parameters are summarized, followed by a discussion of the modeling strategies incorporated in the simulations conducted.

2.1 Archetype Design

To develop the archetype building designs four-story steel braced-frame buildings are designed using current U.S. design provisions: ASCE 7-16, AISC 341-16, AISC 360-16 and analyzed in SAP2000. Fig. 1 provides the basic building plan with dimensions of 91.5 meters (300 feet) by 30.5 meters (100 feet) and a story height of 4.27 meters (12.5 feet). The building has four bays braced with BRBs or hollow structural section SCBFs in each orthogonal direction. Bare steel deck was detailed for the roof based on loads of 2.06 KN/m^2 (42 psf) dead load and 0.96 KN/m^2 (20 psf) live load, and concrete-filled steel deck diaphragms are employed for the floors with 4.07 KN/m^2 (85 psf) dead load and 2.06 KN/m^2 (50 psf) live load. The archetype buildings are assumed to be located in an arbitrary site in Irvine, California, with risk category II and site class D. The design spectral accelerations at short periods and at a 1-second period are 1.030g and 0.569g, respectively. The diaphragm is designed following four different alternatives: (1) **Standard design:** traditional ELF-based diaphragm demands as found in ASCE 7-16 or earlier and in the main body of ASCE 7-16; (2) **Alternative Design 1:** diaphragms are scaled to have the required strength from the

alternative diaphragm design procedures considering no ductility (R_s=1.0); (3) **Alternative Design 2:** procedures with R_s = 2 for concrete-filled steel deck diaphragm and R_s = 2.5 for bare steel deck diaphragm; (4) **Alternative Design 3:** diaphragms that have a strength equal to the nominal strength of the diaphragm design using the alternative diaphragm design procedures considering some ductility (R_s=3.0).

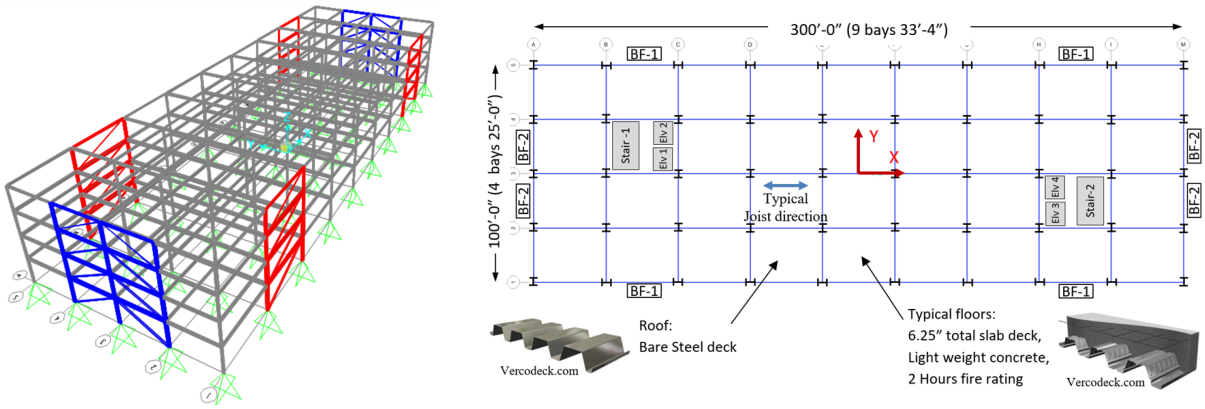

(*a*) (*b*)

Figure 1: Schematic view of four-story archetype building: (a) 3D model, (b) typical plan

For the archetype buildings, the diaphragm design forces in the short direction of the buildings are provided in Table 2. Further details of the archetype buildings and the design process can be found in (Torabian et al. 2017).

2.2 Archetype Simulation

A computational model of the archetype buildings was created in the software, OpenSees, with nonlinear phenomenological elements for the diaphragm and SCBF and BRB braces as detailed in subsequent sections. All columns are pinned at their base. All beam-to-column and beam-to-beam joints are pinned with the exception of the braced bays which use semirigid connections at the beam-to-column joint to simulate the influences of the gusset plates. As recommended by FEMA P695 the gravity loads include a combination of dead and live loads (1.05D+0.25L). Mass was determined from the dead loads and lumped at the column nodes on each floor. For nonlinear response history analysis, Rayleigh damping with a critical damping ratio equal to 2% for the 1st and 4nd mode is used for the archetype building models. Both material and geometric nonlinearity are considered in the analysis, except where otherwise designated in the model results.

The two key nonlinear building components examined herein are the diaphragm and the concentric braces in the frames. These two elements are calibrated using existing data and then appropriately modified for use in the archetype building. Calibration and the modeling details for these building elements are provided in the following two sections.

2.3 Diaphragm Modeling

The archetype building designs employ both bare steel deck and concrete-filled steel deck diaphragms. Existing experiments are used to calibrate accurate nonlinear hysteretic models for the in-plane diaphragm response. The SDII cantilever diaphragm test database was utilized to select appropriate test specimens (O'Brien et al. 2017). For a typical bare steel deck roof

diaphragm Specimen 33 with 20-gage 38.1 *mm* (1.5 *in*). deep B-deck and employing PAFs for the structural connectors and screws for the sidelap connections, based on testing of Martin (2002), was found to have sufficient design strength to match the roof demands, or otherwise scaled, and is herein denoted as SP1. For the alternative design 1 (R_s =1) in the 8 and 12 story archetype buildings with SCBF as the lateral force resisting system, SP1 bare steel deck is not sufficient for the roof demand. To have sufficient design strength to match the roof demands for those archetypes, specimen 12 with 22-gage 38.1 *mm* (1.5 *in*) deep B-deck and welded sidelaps is chosen based on the testing of Essa et al. (2003) herein denoted as SP2. For a typical concrete-filled steel deck test specimen 3/6.25-4-L-NF-DT which consisted of 72.6 *mm* (3 *in*). deck, with lightweight concrete fill and 158.75 *mm* (6.25 *in*) total thickness from Avellaneda et al (2019), herein denoted as SP3 was selected.

The test results are reported from cantilever diaphragm tests as depicted in Fig. 2a. The in-plane response is simulated through nonlinear truss elements as depicted in Fig. 2b. The Pinching4 material model in OpenSees is used for the truss elements to simulate the hysteretic behavior and capture cyclic strength and stiffness degradation behavior of the diaphragms. The parameters of the Pinching4 model are fit to the selected test results employing a multi-level optimization procedure with independent objective functions including cumulative strain energy, peak load, and degradation slopes. Table 1 provides the final calibrated Pinching 4 material parameters including backbone stresses and strains and cyclic strength and stiffness degradation for the two selected diaphragm specimens. A comparison of the hysteretic response from the calibrated diaphragm simulation and that from the experiment is shown in Fig. 3. The dimensions of the archetype building diaphragm units do not directly coincide with those of the test specimens, therefore the strategy described in Qayyum (2017) is adopted to modify the backbone parameters so that the diaphragm shear strength per unit length is consistently represented.

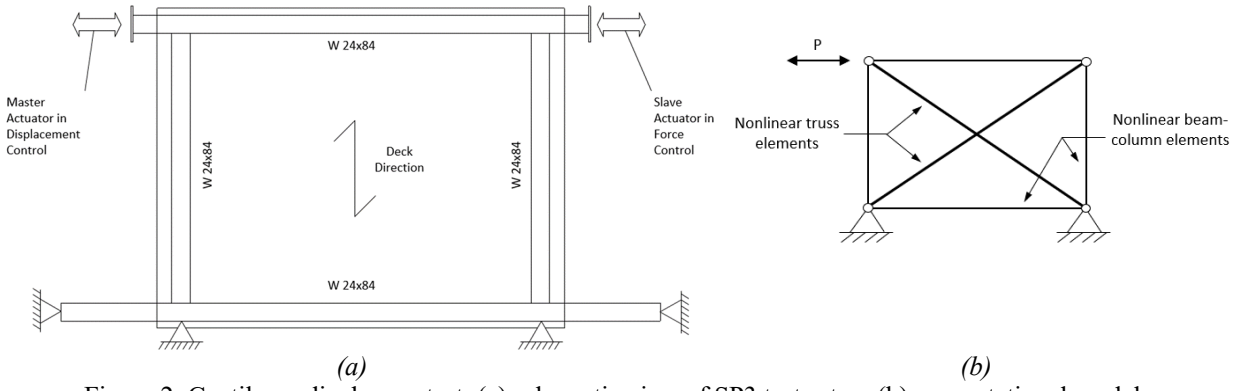

(a) *(b)*

Figure 2: Cantilever diaphragm test: (a) schematic view of SP3 test setup, (b) computational model

Table 1: Calibrated Pinching4 Material Model Parameters

Test	Backbone				Pinching			Strength Degradation					Stiffness Degradation					Energy Dissipation
	ε_1,σ_1 (*MPa*)	ε_2,σ_2 (*MPa*)	ε_3,σ_3 (*MPa*)	ε_4,σ_4 (*MPa*)	r_{Δ^+}, r_{Δ^-}	r_{p^+}, r_{p^-}	u_{Δ^+}, u_{Δ^-}	gF_1	gF_2	gF_3	gF_4	gF_{lim}	gK_1, gD_1	gK_2, gD_2	gK_3, gD_3	gK_4, gD_4	gK_{lim}, gD_{lim}	gE
SP1	0.0008, 152.9 (22.18 *ksi*)	0.0017, 199.2 (28.89 *ksi*)	0.0033, 211.6 (30.69 *ksi*)	0.0053, 165.3 (23.97 *ksi*)	0.20, 0.35	0.20, 0.35	0.10, 0.12	0	0.35	0	0.70	0.90	0, 0	0, 0.50	0, 0	0, 0.75	0, 0.90	4.31
SP2	0.0009, 40.0 (5.80 *ksi*)	0.0015, 53.6 (7.77 *ksi*)	0.0041, 64.0 (9.28 *ksi*)	0.0073, 29.7 (4.31 *ksi*)	0.05, 0.35	0.28, 0.35	0.12, 0.12	0	0.45	0.0	0.50	0.87	0.32, 0.00	0.60, 0.38	0.52, 0.00	1.52, 0.00	1.07, 1.08	2.02
SP3	0.0005, 437.6 (63.46 *ksi*)	0.0006, 526.8 (76.41 *ksi*)	0.0014, 740.5 (107.4 *ksi*)	0.014, 333.2 (48.33 *ksi*)	-0.06, -0.06	0.12, 0.12	0.11, 0.11	0	0.83	0.0	0.46	0.33	1.09, 0.14	0.76, 0.47	0.32, 0.12	0.75, 0.10	1.04, 0.61	4.29

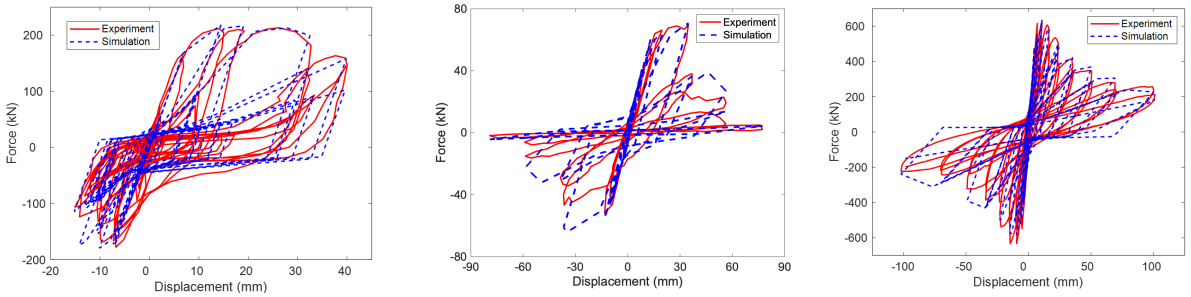

(a) *(b)* *(c)*

Figure 3: Hysteretic response of diaphragm from experiment and simulation: (a) SP1, (b) SP2, (c) SP3

Table 2 provides the calculation for the scale factors of the diaphragm to the Pinching4 backbone strength (as implemented in OpenSees) for the archetype buildings, where V_{r_LRFD} and V_{r_ASD} are the shear demand (per unit width) of the diaphragm using LRFD and ASD, respectively, α is the safety factor for ASD, $v_{n\_Estimated}$ is the expected nominal strength of the diaphragm design, and V_{exp} is the peak strength from experimental hysteretic curve. It should be noted that for all the archetype buildings, shear stud diameter and length are 19.05 *mm* (0.75 *in*) and 144.3 *mm* (4.5 in), respectively. Light weight concrete-filled steel deck is the chosen floor system in the buildings. Concrete thickness is 82.55 *mm* (3.25 *in*) and f'$_c$ is 27.58 MPA (4000 psi) for all the archetypes.

Table 2: Scale factor for the designed diaphragm demand in archetype building

Cases	Diaphrahm Design	Level	V_{Design} (kip/ft)	V_{n_Design} (kip/ft)	$V_{n\_Estimated}$ (kip/ft)	Estimated Limit state	V_{exp} (kip/ft)	Experimental Limit State	Scale Factor
1	Traditional / Rs =2 , Rs =2.5	Roof	1.3	3.3	3.31	Sidelap fasterner	2.45	Sidelap fasterner	1.35
		Floor	3.0	9.6	11.40	Shear stud	9.55	Diag. Tension Cracking	1.19
2	Rs =1	Roof	2.9	8.7	8.70	Connection (Weld)	0.53	Connection (Weld)	16.42
		Floor	4.7	15.4	16.80	Diag. Tension Cracking	9.55	Diag. Tension Cracking	1.76
4	R_s =3	Roof	0.9	2.3	2.07	Sidelap fasterner	2.45	Sidelap fasterner	0.84
		Floor	1.8	5.9	11.4	Shear stud	9.55	Diag. Tension Cracking	1.19
5	Traditional / Rs =3 / Rs =2 , Rs =2.5	Roof	2.1	1.4	2.18	Sidelap fasterner	2.45	Sidelap fasterner	0.91
		Floor	4.9	3.3	11.4	Shear stud	9.55	Diag. Tension Cracking	1.19
6	Rs =1	Roof	1.3	0.9	3.5	Sidelap fasterner	2.45	Connection (Weld)	1.45
		Floor	2.6	1.8	16.79	Diag. Tension Cracking	9.55	Diag. Tension Cracking	1.76

2.4 Brace Modeling

As provided in Fig. 4a, the BRB core (restrained yielding segment) is represented by a nonlinear truss element with Steel4 material model in OpenSees. The non-yielding segments on both ends are modeled with elastic beam-column elements, and another elastic beam-column element with negligible cross-section area and large bending stiffness is also used to connect the non-yielding segments to fix the rotational degrees of freedom and prevent instability of the truss element. The calibration of the BRB core material model has been conducted against test data to match the behavior of specimens tested by Newell et al. (2006). Fig. 4b shows an example for the hysteretic curves of the calibrated model as compared to the test results. The calibrated Steel4 material parameters were used in the archetype building modeling and the values are given in Table 3.

Fatigue material model uniaxialMaterial Fatigue in OpenSees was also calibrated to capture BRB fracture. Only one specimen (as shown in Fig. 4b) fractured during the test by Newell et al. (2016), and therefore its test data were used in the calibration. However, two parameters need to be calibrated: ε_0, the value of strain at which one cycle will cause failure, and m, the slope of Coffin-Manson (Coffin, 1954; Manson, 1954) curve in log-log space. Given only one set of test data, ε_0 was assumed to be 0.2 based on the elongation at break (in 8 in.) of A36 core steel per ASTM standards (ASTM 2019), while m equal to -0.5976 was calibrated such that fracture occurred at the loading point in the simulation close to that in the test.

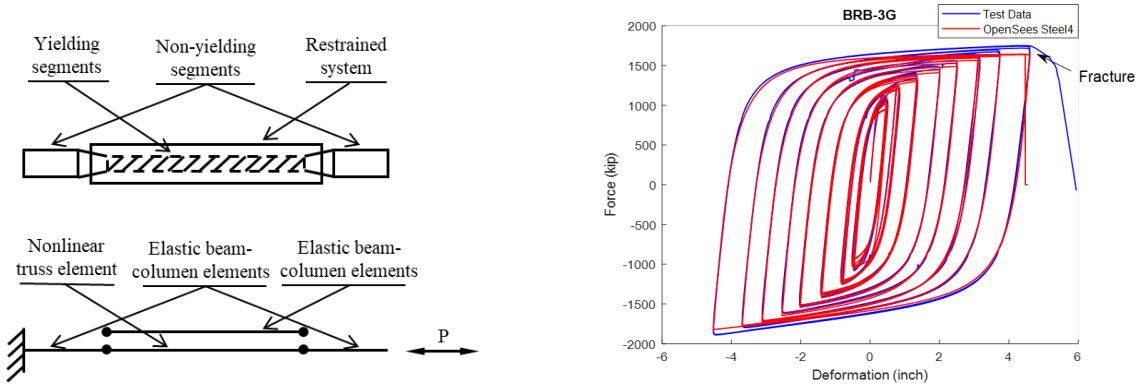

(a) Computational model (b) Calibration of BRB Steel4 material model

Figure 4: Configuration of BRB computational model and example hysteretic curve for BRB Steel4 calibration

Table 3: Calibrated Steel4 Parameters for BRB model

b_k	R_0	r_1	r_2	b_i	b_l	ρ_i	R_i	l_{yp}	f_u	R_u
0	20.9837	0.9122	0.1209	0.0306	0	0.7262	1.3134	18.2022	70.3000	620.6286
b_{kc}	R_{0c}	r_{1c}	r_{2c}	b_{ic}	b_{lc}	ρ_{ic}	R_{ic}	l_{ypc}	f_{uc}	R_{uc}
0.0121	18.9116	0.9133	0.1232	0.0020	0	0.9061	2.9727	37.3548	108.4701	583.5268

Concentric braces are prone to buckle when they are under compression. To employ an accurate model to simulate the CBF behavior in both tension and compression, a computational OpenSees model is developed which is calibrated against experimental results. Fig. 5 shows the detail of the concentric brace model. A hollow structural section (HSS) with rotational springs at two ends is used in the computational model to simulate the rigidity of the gusset plates. Geometric imperfections equal to L/1000 in the shape of a single half-sine wave are included, and the brace is discretized into eight elements along its length. Two Zerolength elements have been used at the two ends of the brace to assign the rotational springs. Fiber elements are used for the brace with 3 fibers through the thickness and 16 fibers along each side of the HSS (see Fig. 5). The calibration of the SCBF material model has been conducted against test data to match the behavior of specimens tested by Popov and Black (1981) and Fell et al. (2009). For Popov and Black (1981), no rotational springs were used at the ends because there was a true pin. Table 4 presents the Steel02 material model and rotational spring parameters for the three different studies. As can be seen in Fig. 5, the model can capture the behavior of the brace in both tension and compression.

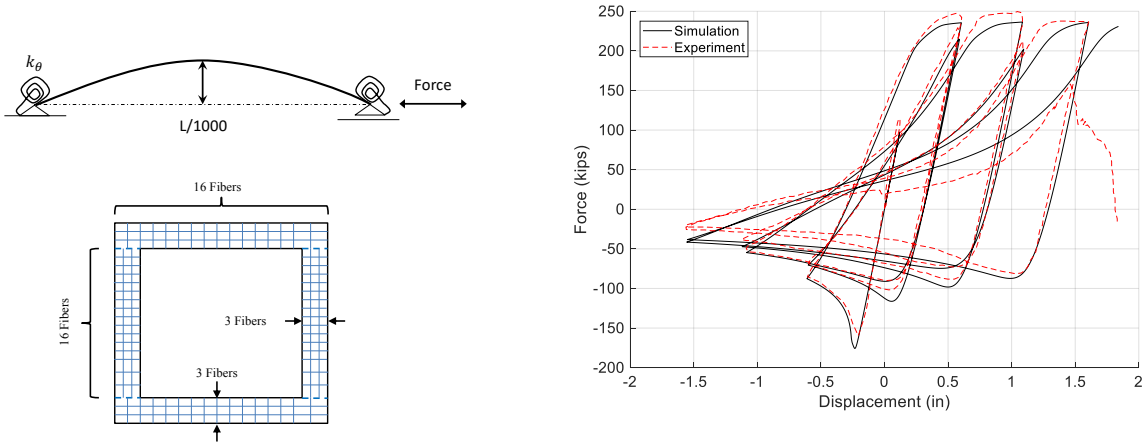

(a) *(b)*

Figure 1: *(a)* Configuration of a typical SCBF and computational model *(b)* experiment and simulation (Fell et al. (2009) Specimen HSS 1-1)

Table 1: Calibrated Steel02 and Rotational Spring Parameters for SCBF

SCBF material	**F_y (ksi)**	**b**	**R0**	**CR1**	**CR2**	**a1**	**a2**	**a3**	**a4**	**-**
	70.2	0.005	20.1	0.90	0.15	0	1	0	1	-
Rotational Springs	**M_y (k-in)**	**K_{spring}**	**R0**	**CR1**	**CR2**	**a1**	**a2**	**a3**	**a4**	**Harden**
	414	0.002	20	0.9	0.15	0	1	0	1	0.005

EqualDOF constraints are applied at the brace ends with all DOF's constrained except for the buckling rotation. To capture the effects of fracture in the SCBF model the MINMAX material is used in OpenSees. Fracture strain is recorded using OpenSees by tracking the strain value in the fibers. Fracture strain is set to 0.05 in the models. Note, this model of the brace neglects explicit modeling of local buckling effects.

4. Analysis Results

Models of the developed SCBF and BRB steel-framed archetype buildings were used to conduct modal analysis, static pushover analysis, and nonlinear time history analysis. The impact of different vertical lateral force resisting system and diaphragm design are examined herein.

4.1 Eigenvalue Analysis

The fundamental mode shapes and frequencies for the Archetype building model were calculated. Fig. 6 shows the different typical mode shapes observed in the analyses. Table 5 provides the first three periods and mode shapes for the different design archetypes. The difference between the OpenSees result and the SAP model (rigid diaphragm, used in archetype design) provides a measure of the contribution of the diaphragm flexibility to the model results.

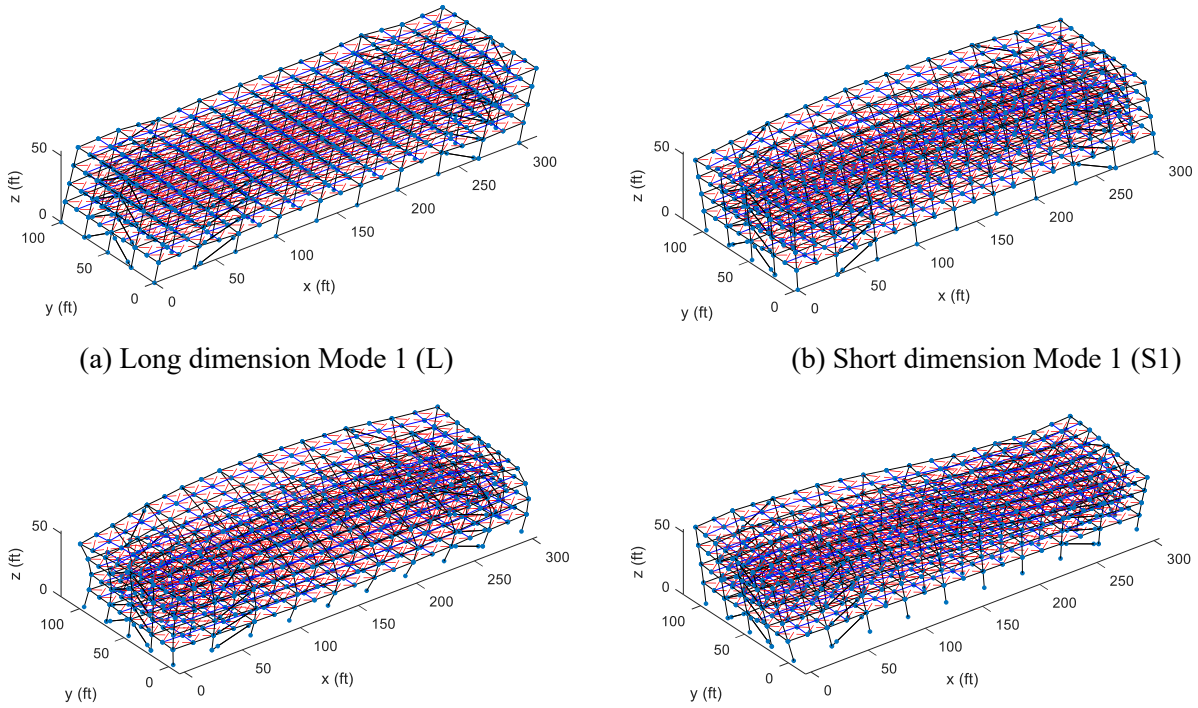

(a) Long dimension Mode 1 (L)

(b) Short dimension Mode 1 (S1)

(c) Short dimension Mode 2 (S2)

(d) Torsional mode (T)

Figure 6: Example mode shapes of four-story BRB archetype models

Table 5: Natural Periods of Archetype Buildings

Building Model	Diaphragm Design	T1 (sec)	Mode Type	T2 (sec)	Mode Type	T3 (sec)	Mode Type
4-story BRB	Rigid Diaphragm	0.94	L	0.76	S1	0.48	T
	Traditional / Alt. R_s = 2-2.5	1.17	L	1.17	S1	0.74	S2
	Alt. R_s = 1	1.16	L	1.12	S1	0.69	S2
4-story SCBF	Rigid Diaphragm	0.70	S1	0.69	L	0.42	T
	Traditional / Alt. R_s = 2-2.5	0.81	S1	0.72	L	0.46	S2
	Alt. R_s = 1	0.76	S1	0.70	L	0.44	S2
	Alt. R_s = 3	0.83	S1	0.73	L	0.48	S2

4.2 Static Pushover Analysis

Pushover analysis was conducted to study the static behavior of the archetype building. A displacement-controlled load pattern was applied to the structure in the short direction of the building. Per FEMA P695, vertical distribution of the lateral force at each node was assigned proportional to the product of the tributary mass and the fundamental mode shape coordinate at the node obtained from eigenvalue analysis in OpenSees. Fig. 7 shows the pushover curves obtained from the analysis.

It can be observed that the different diaphragm designs had little effect on the pushover behavior because the pushover analyses used a first mode shape based load pattern and as such were dominated by inelasticity in the vertical bracing system. For the BRB buildings, the first point of nonlinearity on the pushover curves is associated with yielding of the BRB cores, followed by a hardening segment with reduced slope, which is related to the stiffness provided by the BRB frames before hinging occurs at the beam-to-column connections. Once the beam-to-column connections starts to develop plastic hinges, softening response occurs due to P-Δ effect (note that the analysis for BRB building with Traditional / Alternative 2 diaphragm design failed to converge before secondary softening occurred). For the SCBF building, the failure mode is dominated by buckling and yielding in SBCF braces for all three designs. As is shown in Fig. 7, the stiffness of the SCBF decreases slightly due to buckling of the braces in compression. After the first yielding of the tension braces, maximum strength is reached due to P-Δ effect. The analysis ended by the loss of rigidity at the beam-to-column connections in the first floor of the building.

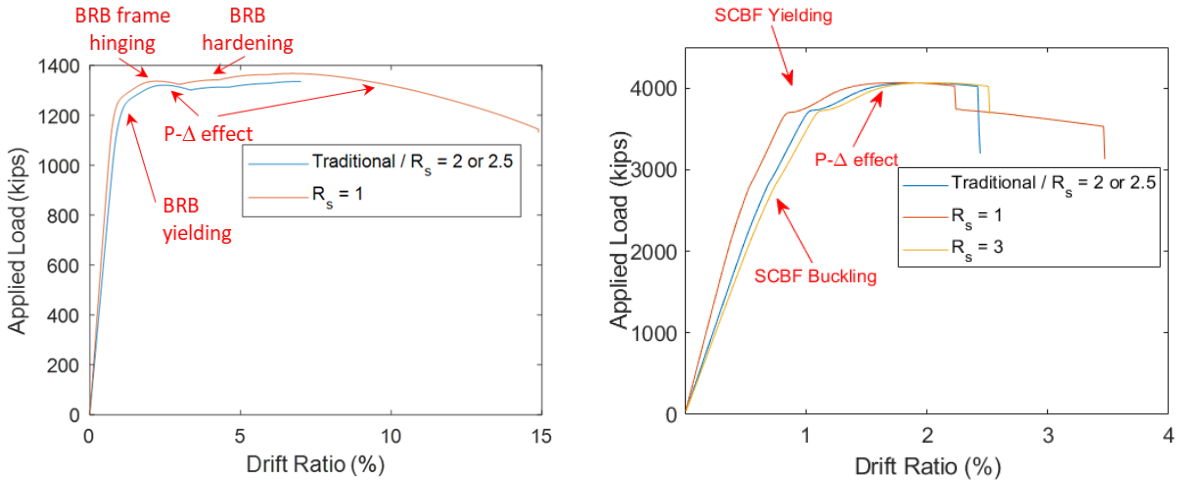

(a) *(b)*

Figure 7: Nonlinear pushover analysis for 4 -story archetype: (a) BRB building, (b) SCBF building

In Table 6, period-based ductility (μ_T) and overstrength (Ω) are obtained from pushover analyses for the short direction of the archetype buildings. The period-based ductility (μ_T) defined as the ratio of the post-peak roof displacement ($\delta_{u\,80\%}$), at the point of 20% strength loss ($0.8P_{max}$) to the effective yield roof displacement ($\delta_{y,eff}$), which can be obtained using Equation B-2 in FEMA P695. For the models with convergence issues, the roof displacement in the last step of analysis (δ_u) is used instead of the post-peak roof displacement ($\delta_{u\,80\%}$). The overstrength (Ω) of the

building is calculated by dividing the peak load by the design base shear. Table 6 shows the values for the ductility and overstrength. We can see that overall the building with the BRB system has smaller overstrength but much larger ductility than the building with SCBF system.

Table 6: Overstrength and period-based ductility for archetype buildings

Building Model	Diaphragm Design	Design Shear (Vb) (kips)	Short Direction	
			Overstrength (Ω)	Ductility (μ_T)
4-story BRB	Traditional / Alt. R_s = 2-2.5	830	1.61	10.65
	Alt. R_s = 1		1.65	23.37
4-story SCBF	Traditional / Alt. R_s = 2-2.5	1529	2.66	3.80
	Alt. R_s = 1		2.67	5.33
	Alt. R_s = 3		2.66	2.98

4.2 Nonlinear Time History Response Analysis

To evaluate the seismic performance of the archetype buildings and various diaphragm designs, nonlinear response time history analysis was performed with the building model subjected to the FEMA P695 suite of far-field earthquake motions. To represent different hazard levels in nonlinear response history analysis (NRHA), 22 pairs of ground motion records from the FEMA P695 far-field record suite are scaled to three different intensities: 1) Design Earthquake (DE); 2) Maximum Considered Earthquake (MCE) and 3) A scale level based on adjusted collapse marginal ratio ($ACMR_{10\%}$). For DE and MCE, the ground motions are scaled such that the median spectrum matches the design spectrum at the fundamental period of the building. To be consistent with FEMA P695 methodology, the value of the fundamental period for each archetype building is obtained by the product of the coefficient for upper limit on calculated period (C_u) and the approximate fundamental period (T_a) as defined in ASCE 7-16 Section 12.8.2. The third scale level is related to median collapse for acceptability according to FEMA P695. The scale factor was obtained with the method is described in Appendix F.3 of FEMA P695: first an acceptable value of adjusted collapse margin ratio ($ACMR_{10\%}$) is obtained with assumed total system collapse uncertainty; then the period-based ductility (μ_T) is obtained from the pushover analysis; and finally the spectral shape factor (SSF) and the collapse marginal ratio (CMR) is obtained. The scale factor based on $ACMR_{10\%}$ is then obtained by multiplying the collapse marginal ratio by the scale factor for MCE.

Consider first the BRB building, Fig. 8 shows example response history results with peak story drift, BRB hysteresis, and diaphragm truss hysteresis of the 4-story BRB building with Traditional / Alternative 2 diaphragm design subjected to the 1995 Kobe Earthquake ground motion at DE, MCE, and $ACMR_{10\%}$ levels. We can see that while the peak story drift of the building subjected to DE-level ground motion remains relatively small (less than 3%), under the MCE-level ground motion it has peak story drift larger than the 10% limit, and under $ACMR_{10\%}$-level ground motion it experiences ever increasing story drifts, which both indicate that the building collapses. The BRB's and diaphragms all undergo some inelastic deformation for all three levels of ground motions. For BRB's, the hysteresis curves show that energy is successfully dissipated by the BRB inelastic deformation, but at the $ACMR_{10\%}$ level, excessive BRB deformation occurs and causes the building to collapse. Floor diaphragms remain relatively elastic compared to the roof diaphragms under the DE and MCE-level ground motions, whereas for $ACMR_{10\%}$ level, the floor diaphragms are affected by the large story drift due to the excessive deformation of the BRB and also undergo large deformation, which may be caused by computational errors as the analysis results became inaccurate after large deformation occurred with building collapse.

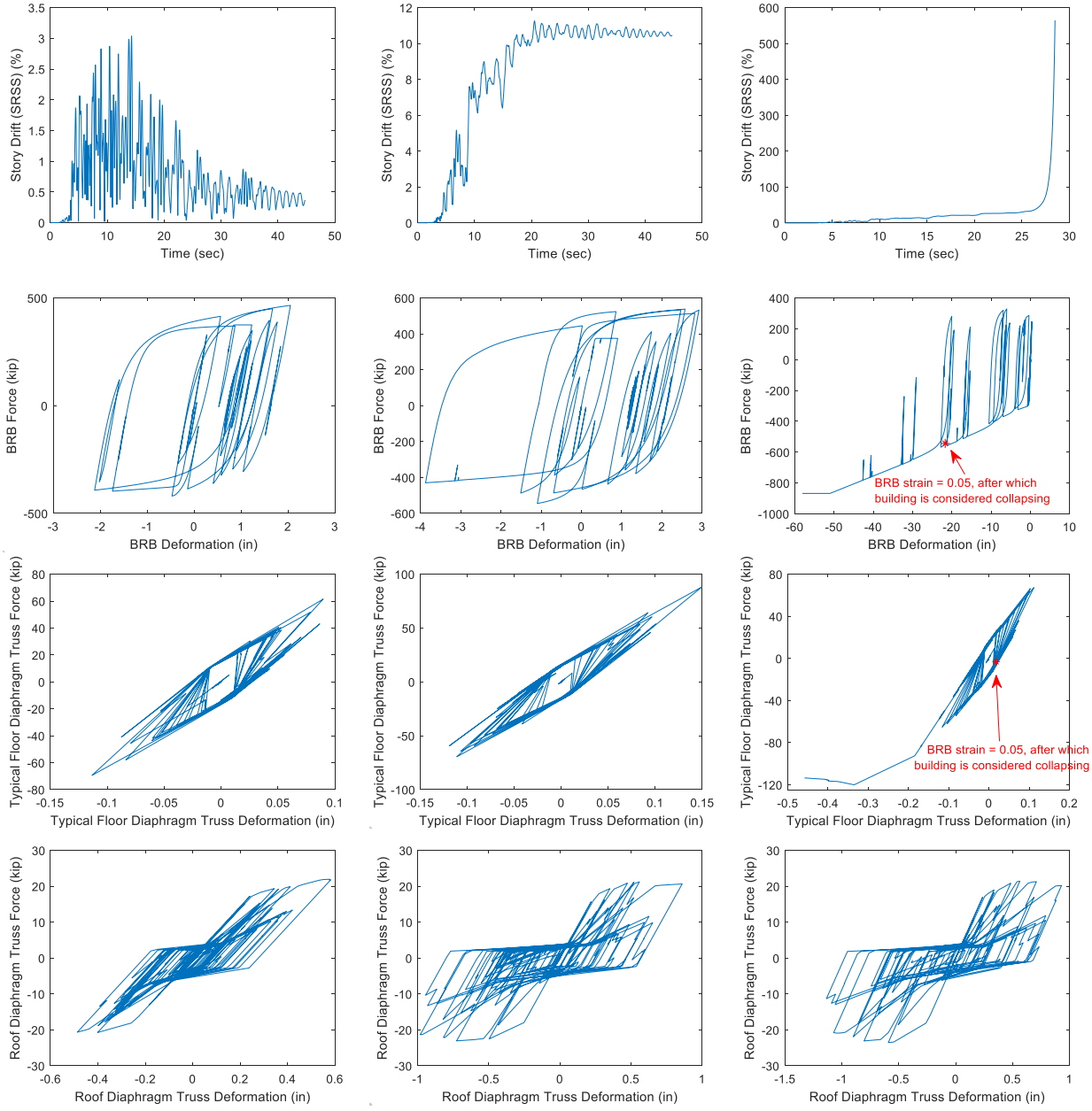

(*a*) DE (*b*) MCE (*c*) $ACMR_{10\%}$

Figure 8: Time history response of 4-story building with the Traditional / Alternative 2 diaphragm design under three levels of ground motions (from top to bottom: peak story drift, base story BRB hysteresis, floor diaphragm truss hysteresis, roof diaphragm truss hysteresis)

For the SCBF building Fig. 9 indicates similar response history results to Fig. 8 now for the 4-story SCBF building with Traditional / Alternative 2 diaphragm design. The peak story drift remains small for DE and MCE-level ground motion, but under $ACMR_{10\%}$-level ground motion the peak story drift exceeds 10% which indicates that the building has a high probability of collapse. The SCBF building experiences buckling and yielding in the braces. However, hysteresis curves show less dissipated energy compared to the BRB braces, as expected. The bare steel deck roof

diaphragms experience larger deformations and more inelasticity than the concrete-filled steel deck floor diaphragms. For the $ACMR_{10\%}$ level, large deformation along with inelastic response of the diaphragm typically causes collapse in the SCBF building as the gravity columns lose their support. This is in contrast to many of the BRB buildings where large deformation in the BRB's cause large story drift and potentially collapse.

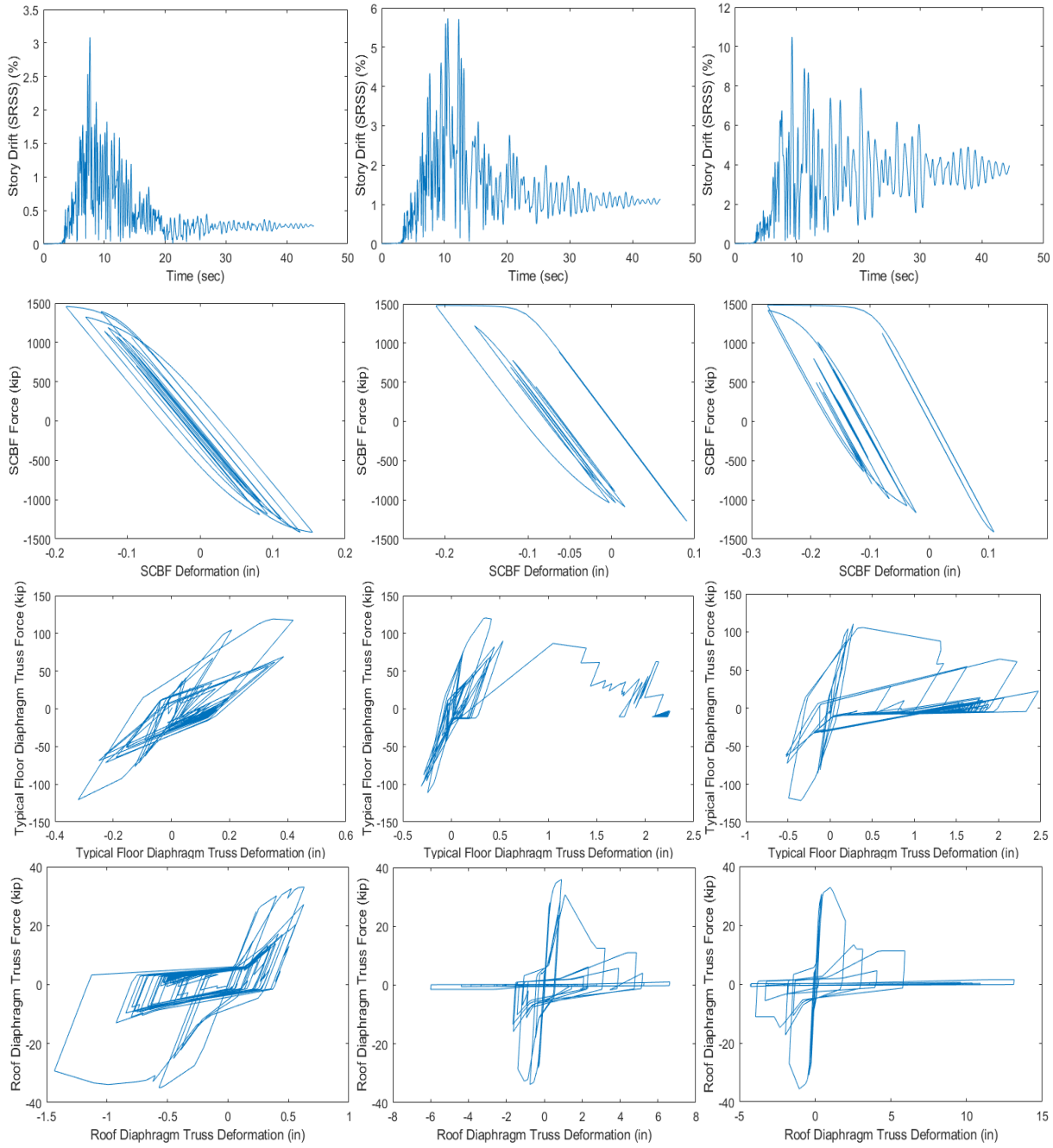

(*a*) DE (*b*) MCE (*c*) $ACMR_{10\%}$

Figure 9: Time history response of 4-story building with the Traditional / Alternative 2 diaphragm design under three levels of ground motions (from top to bottom: peak story drift, base story SCBF hysteresis, floor diaphragm truss hysteresis, roof diaphragm truss hysteresis)

To illustrate the deformation demand of the diaphragms and brace system of the building, the contour of normalized diaphragm shear angle demand and brace strain demand are plotted in Fig. 10 and Fig. 11 for the 4-story buildings with different diaphragm designs at the MCE level. The normalized diaphragm shear angle demand is determined by the maximum diaphragm shear angle experienced by each of the diaphragm units throughout the time history divided by γ_1, which is the shear angle reached when the diagonal trusses of the diaphragm unit undergo an axial strain equal to ε_1 of the Pinching4 parameters given in Table 1. The normalized strain demand of each BRB is obtained by dividing the maximum axial strain of the BRB throughout the time history by ε_y, which is the yield strain of the BRB given by $\varepsilon_y = F_y/E$ where F_y is the yield stress of the BRB and E is the elastic modulus of steel. Similarly, for the SCBF, the normalized strain demand of each brace is obtained by dividing the maximum axial strain of the braces in tension throughout the time history by ε_y, which is the yield strain of the SCBF. It can be observed from Fig. 10 that all the BRB's experienced inelastic deformation while the braces remain largely elastic for the SCBF buildings, see Fig. 11. The diaphragm shear angle demand of the BRB building with Traditional / Alternative 2 diaphragm design was larger than that of the building with Alternative 1 design. Inelastic deformation occurred in the bare steel deck roof diaphragm, while the concrete-filled steel deck floor diaphragms with Traditional / Alternative 2 design exhibited some inelastic deformation demand. As can be seen in Fig 11, the diaphragm shear angle demand of the SCBF building was larger for Alternative 3 design compared to Traditional / Alternative 2. For Alternative 1 design, diaphragm shear angle demand is small. Inelastic deformation occurred in the bare steel deck roof and concrete-filled steel deck floor diaphragm for all three designs.

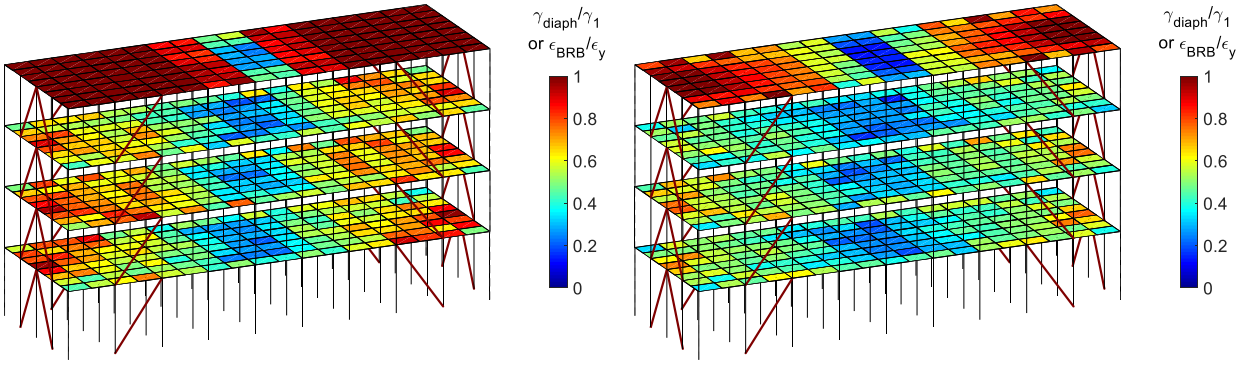

(a) Traditional / Alternative 2 (b) Alternative 1

Figure 10: Contour of normalized diaphragm shear angle demand and normalized BRB strain demand of 4-story BRB building with different diaphragm designs under MCE-level ground motions

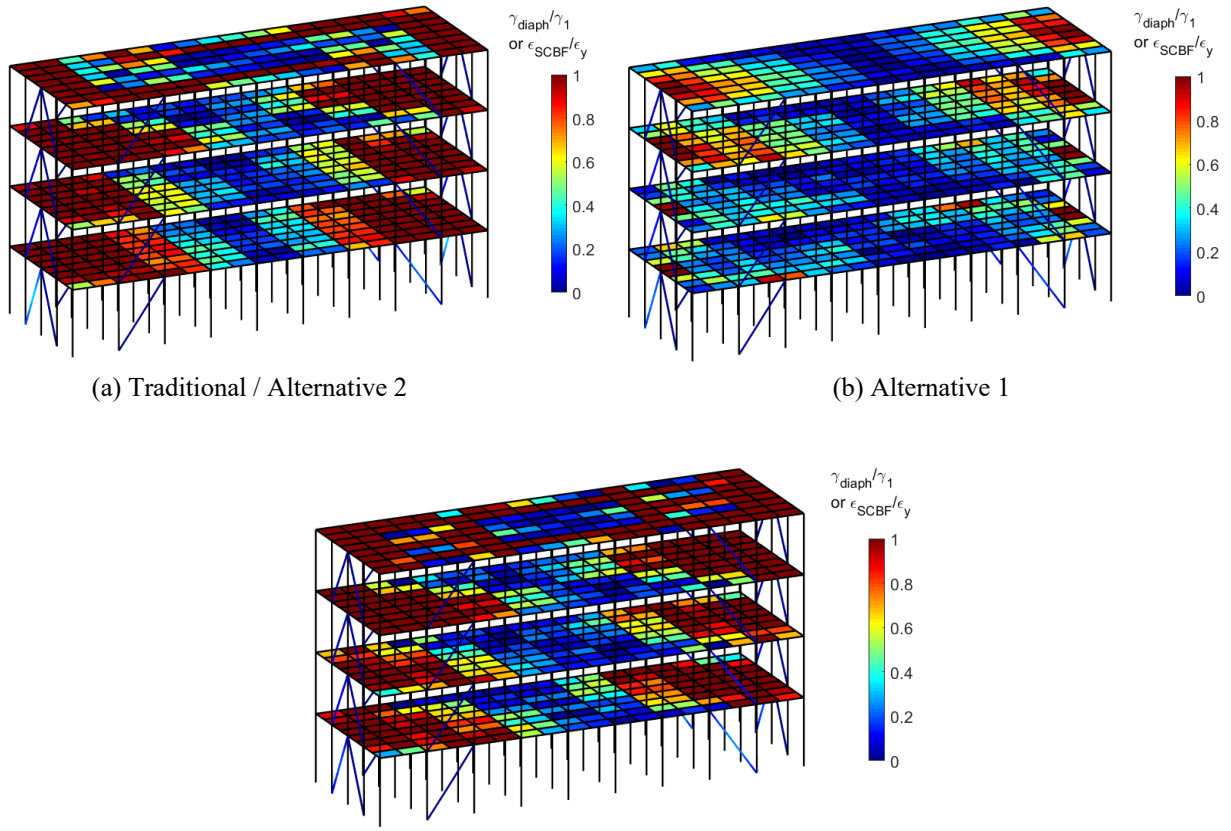

(a) Traditional / Alternative 2

(b) Alternative 1

(c) Traditional / Alternative 2

Figure 11: Contour of normalized diaphragm shear angle demand and normalized SCBF strain demand of 4-story SCBF building with different diaphragm designs MCE-level ground motions

To investigate the seismic performance (collapse prevention) of the archetype buildings, collapse ratios, i.e., probabilities of collapse, were calculated for each set of runs of nonlinear response history analysis. For the definition of building collapse, there are three criteria considered:

- maximum story drift ratio exceeds 10%;
- maximum diaphragm shear angle exceeds 4%, this limit is determined based on the evaluation of the cantilever diaphragm test database and connector tests; and
- convergence failure occurs in the analysis - for those analyses that fail to converged, whether the building collapses is first checked against criteria 1) and 2), if neither of these two criteria is met, it is then determined on a case-by-case basis.

Table 7 provides the collapse ratios for all the archetype buildings.

Table 7 Collapse ratios for buildings under three levels of ground motions

Archetype Building		DE	MCE	$ACMR_{10\%}$
4-story BRB	Trad. /Alt. 2	6.8%	20.5%	31.8%
	Alt. 1	2.3%	13.6%	27.3%
4-story SCBF	Alt. 3	32.1%	70.2%	90.0%
	Trad. /Alt. 2	0.0%	20.3%	41.4%
	Alt. 1	0.0%	0.0%	9.20%

From Table 7 at the $ACMR_{10\%}$ level traditional diaphragm design, R_s=2/2.5 diaphragm design (Alt.2), and R_s=1 elastic diaphragm design (Alt. 1) are acceptable (<50% collapse probability) for

both the BRB and SCBF buildings. However, the R_s=3 diaphragm design (Alt. 3) for the SCBF building has unacceptable collapse probabilities and demonstrates that if the diaphragm forces are reduced too far then the diaphragm failure and consequent loss of support for the gravity columns will drive the building collapse. It is worth noting that use of elastic-level forces for the diaphragm (Rs=1 / Alt. 1) has acceptable, but overly conservative levels of predicted collapse and can be deemed unnecessarily inefficient and cost ineffective. It is worth noting that even though traditional diaphragm design and Rs=2/2.5 diaphragm design (Alt. 2) are deemed acceptable at the ACMR10% level, the failure probability at MCE level is higher than desired (10%). The two building types arrive at similar collapse probabilities despite using different R values in design, different overstrength, and different mechanisms for energy dissipation.

5. Conclusions

The seismic performance of steel braced frames depends on the nonlinear performance of both the vertical and horizontal lateral force resisting systems. ASCE 7 has introduced a new design approach for concrete and wood diaphragms. Appropriate provisions for steel diaphragms are not yet available. Three-dimensional OpenSees models of four-story steel special concentric braced frames (SCBF) and buckling restrained braced (BRB) frame buildings with concrete-filled steel deck floors and bare steel deck roofs are explored. The models are developed based on archetype designs that consider various design approaches for the floor and roof diaphragms including traditional design, elastic design (R_s=1), and inelastic diaphragm design (R_s=2/2.5 or 3). The models include nonlinearity in the braced frames, as well as in the in-plane diaphragm response. Pushover response demonstrates brace yielding and a degrading slope directly attributed to the increasing P-Δ demands. Nonlinear time history response provides more nuanced behavior. Both the braces and the diaphragms contribute to the building response. For BRB buildings the inelasticity and ultimately any collapses are largely driven from the BRB behavior and sensitivity to the diaphragm design is minor. For the SCBF buildings significant inelasticity occurs in the diaphragms, collapse is largely driven by loss of diaphragm support to gravity columns, and the building behavior is sensitive to the design assumptions used for the diaphragm. For the studied four-story BRB and SCBF buildings the collapse probability following traditional ASCE 7 based design, or that using the alternative diaphragm design method with R_s=2 for concrete-filled steel deck and R_s=2.5 for bare steel deck are found to have acceptable levels of collapse. Additional archetype studies, detailed analysis of the collapse mechanisms and the role of P-Δ effects, and further comparisons to current design methods are all underway.

Acknowledgments

This work was supported by the National Science Foundation under Grant No. 1562669, 1562821, and 1562490 as well as he Steel Diaphragm Innovation Initiative which is funded by the American Institute of Steel Construction, the American Iron and Steel Institute, the Steel Deck Institute, the Steel Joist Institute, and the Metal Building Manufacturers Association. Any opinions expressed in this paper are those of the authors alone, and do not necessarily reflect the views of the National Science Foundation or other sponsors.

References

AISC. (2016). “Specification for structural steel buildings, (AISC 360-16) ”,*American Iron and Steel Institute*.

American Society of Civil Engineers. (2010). “Minimum design loads for buildings and other structures (ASCE standard)”, Reston, Va. *American Society of Civil Engineers*.

ASTM. (2019). Standard Specification for Carbon Structural Steel, (ASTM A36 / A36M-19). *ASTM International*, West Conshohocken, PA, 2019, www.astm.org

Avellaneda Ramirez, R.E., Easterling, W. S., Schafer, B.W., Hajjar, J.F., and Eatherton, M.R. (2019) "Cyclic Testing of Composite Concrete on Metal Deck Diaphragms Undergoing Diagonal Tension Cracking", *12th Canadian Conference on Earthquake Engineering*, Chateau Frontenac, Quebec, QC.

Coffin, L.F. (1954). "A study of the effects of the cyclic thermal stresses on a ductile metal", Translat. ASME, 76, 931-950.

EERI. (1996). "Northridge Earthquake Reconnaissance Report", Vol. 2 Earthquake Spectra - Supplement C to Volume 11 Earthquake Engineering Research Institute.

FEMA. (2009). Quantification of building seismic performance factors, (FEMA P695). Applied Technology Council, Federal Emergency Management Agency.

Fell, B.V., Kanvinde, A.M., Deierlein, G.G., Myers, A.T. (2009). "Experimental investigation of inelastic cyclic buckling and fracture of steel braces." *Journal of structural engineering*, 135(1) 19-32.

Han, S.W., Kim, W.T., Foutch, D.A. (2007). "Seismic behavior of HSS bracing members according to width–thickness ratio under symmetric cyclic loading.", *Journal of Structural Engineering*, 133(2) 264-273.

Manson, S.S. (1954). "Behaviour of Materials under Conditions of Thermal Stress", NACA TN-2933. *National Advisory Committee for Aeronautics*.

Martin, É. (2002). "Inelastic response of steel roof deck diaphragms under simulated dynamically applied seismic loading", Master's thesis, *Ecole Polytechnique de Montreal*.

Newell J, Uang CM, Benzoni G. (2006). Subassemblage testing of core brace buckling restrained braces (G Series). University of California San Diego. Report no. TR2006/01; 2006

O'Brien, P., Eatherton, M. R., & Easterling, W. S. (2017). "Characterizing the load-deformation behavior of steel deck diaphragms using past test data", *Cold-Formed Steel Research Consortium Report Series*, CFSRC R-2017-02.

Popov, E. P., Black, R. G. (1981). "Steel struts under severe cyclic loadings.", *Journal of the Structural Division*, 107(9) 1857-1881.

Qayyum, B. (2017). "Computational modeling of one-story buildings with nonlinear steel deck diaphragms subjected to earthquakes." Report, *Virginia Tech*.

Rodriguez, M., Restrepo, J., and Blandón, J. (2007). "Seismic design forces for rigid floor diaphragms in precast concrete building structures", *Journal of Structural Engineering*, 133(11), pp. 1604–1615.

Torabian, S., Eatherton, M.R., Easterling, W.S., Hajjar, J.F., Schafer, B.W. (2019). "SDII Building Archetype Design v2.0", *CFSRC Report R-2019-04*, jhir.library.jhu.edu/handle/1774.2/62106.